

# DESY SUMMER STUDENT PROJECT



## Study of $\epsilon$ -Fe<sub>2</sub>O<sub>3</sub> nanoparticles using high-energy X-ray diffraction

**Lenka Kubíčková**

Charles University in Prague  
Czech Republic

*Area of research:*  
Photon Physics, Material Science



*Supervisor:*

Dr. Jozef Bednarcík  
Deutsches Elektronen Synchrotron DESY  
Notkestr. 85  
22607 Hamburg, Germany  
email: [jozef.bednarcik@desy.de](mailto:jozef.bednarcik@desy.de)  
phone: +49-40-89981861

## Abstract

The main aim of this research project is to determine the temperature dependence of lattice parameters of  $\varepsilon$ -Fe<sub>2</sub>O<sub>3</sub> nanoparticles along with the thermal stability at atmospheric pressure. Two samples (bare nanoparticles and nanoparticles in silica matrix) were measured using the high-energy X-ray beam at the High Resolution Powder Diffraction Beamline P02.1 at PETRA III synchrotron in DESY, Hamburg.



## Contents

<b>1</b>	<b>Introduction and scientific background</b>	<b>1</b>
<b>2</b>	<b>Goals of the research project</b>	<b>1</b>
<b>3</b>	<b>Experimental part</b>	<b>1</b>
3.1	Preparation of samples . . . . .	1
3.2	X-ray diffraction experiments . . . . .	2
3.3	Data analysis . . . . .	3
<b>4</b>	<b>Results and Discussion</b>	<b>4</b>
4.1	Calibration . . . . .	4
4.2	SBA-G57Fe1050-matrix . . . . .	4
4.3	SBA-G57Fe1050-NC1 . . . . .	7
<b>5</b>	<b>Conclusions</b>	<b>7</b>
	<b>Acknowledgement</b>	<b>10</b>
	<b>References</b>	<b>10</b>

## 1 Introduction and scientific background

Magnetic nanoparticles have been in focus of material research for decades. Apart from technological applications including catalysts, solar cells, optical filters or sensor devices, they have found broad applications in medicine, in particular for cell targeting and drug transport, and as contrast agents in MRI. Among magnetic nanoparticles, nanosized iron oxides have attracted considerable attention due to their numerous application-promising properties [1].

As a metastable phase of the ferric oxide with a rare natural occurrence,  $\epsilon$ -Fe<sub>2</sub>O<sub>3</sub> has been prepared in the form of nanoparticles, nanorods, nanowires or a thin film. It exhibits an orthorhombic crystal structure with a space group  $Pna2_1$  with four magnetic sublattices [2]. Owing to its high coercivity of  $\sim 2$  T and multiferroic behavior,  $\epsilon$ -Fe<sub>2</sub>O<sub>3</sub> is a material with a high application potential e.g. in magnetic recording and information storage media, magnetic field-tuneable devices, or in electronic devices intended for high-speed wireless communication.

High-energy X-ray powder diffraction has proven to be a convenient method to determine the crystal structure and lattice parameters of nanoparticles, as well as to investigate slight changes in interatomic distances related to thermal expansion or strains affecting the nanoparticles.

## 2 Goals of the research project

X-ray powder diffraction (XRD) experiments were set up in order to investigate the temperature dependence of lattice parameters of  $\epsilon$ -Fe<sub>2</sub>O<sub>3</sub> nanoparticles in the form of bare nanoparticles and nanoparticles in silica matrix.

Particular tasks of the proposed project for both investigated samples can be summed up as follows:

- perform XRD experiments on studied material in the temperature interval 20 – 700 – 20 °C,
- determine the lattice parameters of  $\epsilon$ -Fe<sub>2</sub>O<sub>3</sub> nanoparticles and their temperature dependence,
- master all related software at the sufficient level required for collecting, processing and publishing experimental data.

## 3 Experimental part

### 3.1 Preparation of samples

Preparation of  $\epsilon$ -Fe<sub>2</sub>O<sub>3</sub> nanoparticles enriched in <sup>57</sup>Fe isotope (sample SBA-G57Fe1050-NC1) consisted of the following steps:

1. preparation of mesoporous amorphous SiO<sub>2</sub> template,
2. impregnation of this template by aqueous solution of iron(III) nitrate nonahydrate (Fe(NO<sub>3</sub>)<sub>3</sub> · 9 H<sub>2</sub>O) enriched in <sup>57</sup>Fe isotope,
3. annealing at temperatures of about 1050 °C
4. leaching off the silica by NaOH.

Preparation of the sample SBA-G57Fe1050-matrix included steps 1, 2 and 3. Figures 1 and 2 show pictures of both samples obtained from transmission electron microscope.

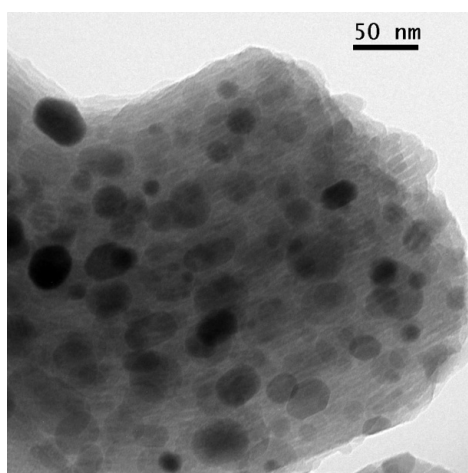


**Figure 1:** TEM picture of SBA-G57Fe1050-matrix - nanoparticles in silica matrix

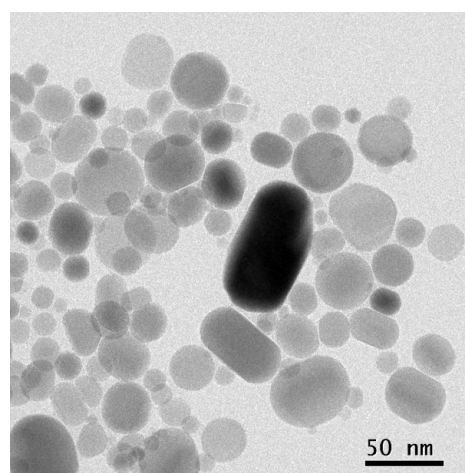


**Figure 2:** TEM picture of SBA-G57Fe1050-NC1 - bare nanoparticles

### 3.2 X-ray diffraction experiments

Powder diffraction experiments were conducted using very brilliant hard X-ray beam of the beamline P02 at PETRA III synchrotron (DESY in Hamburg), specifically of the High-Resolution Powder Diffraction Beamline (HRPD) P02.1. This beamline is dedicated to High Resolution Powder Diffraction (HRPD) experiments at ambient pressure and high/low temperatures at a fixed photon energy of 60 keV (corresponding to the wavelength of 0.207 Å). Diffracted photons are detected using fast area detector PerkinElmer XRD1621 with the active area of 40 × 40 cm<sup>2</sup> consisting of 2048 × 2048 pixels. The beamline is equipped with devices enabling measurements in various sample environments, e.g. Hot-Air-Blower, Cryostreamer, Lamp Furnace or Linkam Furnace.

Samples examined in this project were measured at ambient pressure and atmosphere in quartz capillaries with diameter of 0.4 mm, spinning around the longitudinal axis. A detail of the experimental setup is shown in Figure 3, Figure 4 shows the silicon calibrant in the capillary during the experiment. Heating of the samples and thermal stabilization were provided by the Hot-Air-Blower, each sample was measured during

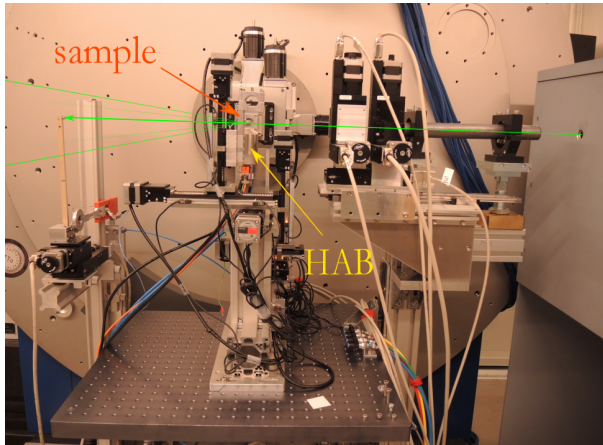


**Figure 3:** Detail of the experimental setup with the position of the sample and the Hot-Air-Blower (HAB), the incoming beam depicted in green colour is absorbed by the beam-stop, diffracted X-rays are caught by the detector PerkinElmer, which is not included in the picture.



**Figure 4:** Silicon calibrant in a spinning capillary during the experiment,  $T_{HAB} = 1000^\circ\text{C}$

the process of heating from  $20^\circ\text{C}$  to  $700^\circ\text{C}$  with subsequent cooling back to  $20^\circ\text{C}$ . The temperature was changed stepwise (Figure 5, detail in Figure 6) with steps of  $20 - 50^\circ\text{C}$  between measurements. Samples were illuminated for 30 seconds, and two shots were taken at selected temperatures. Temperature calibration was performed using silicon standard reference in a spinning quartz capillary with 0.4 mm in diameter in the temperature interval  $20^\circ\text{C} - 1000^\circ\text{C}$  with steps of  $50^\circ\text{C}$ . Silicon calibrant was also used to determine the sample-to-detector distance and other integration parameters with respect to the incoming beam. To determine the background of measurements mentioned above, a diffraction pattern of an empty capillary at the room temperature and an ambient atmosphere was also taken.

### 3.3 Data analysis

Diffraction pattern data obtained during the experiments in the form of .tif files were integrated in the Fit2D software [3], using the polar coordinate system with the origin at the centre of the beam determined by the calibration to silicon standard. During the integration process, background was subtracted with a proper weighting coefficient and bad pixels were omitted.

Peaks in the diffractograms were assigned to Miller indices using the Powder Cell for Windows software [4]. Lattice parameters of a given phase of the ferric oxide were found by fitting peaks inside a chosen interval of  $2\theta$  in the diffractograms with respect to its crystal system. Profiles of diffraction peaks were fitted by Pseudo-Voigt function. The fitting of the data and graphical outputs presented in this report were carried out in Gnuplot [5].

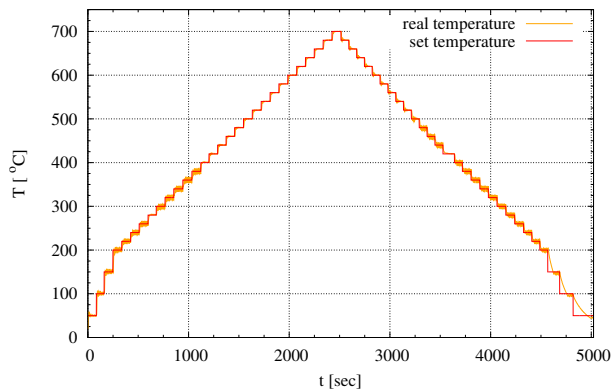


**Figure 5:** Time dependence of the temperature set and achieved during the experiment (SBA-G57Fe1050-NC1)

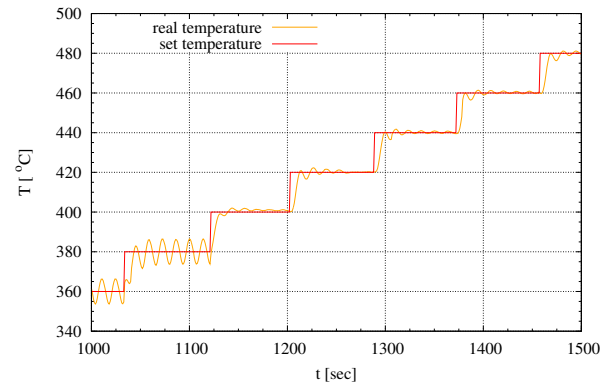


**Figure 6:** Time dependence of the temperature set and achieved during the experiment - detail of the temperature stabilization (SBA-G57Fe1050-NC1)

## 4 Results and Discussion

### 4.1 Calibration

According to the temperature calibration the real temperature of the sample was higher than the temperature  $T_{HAB}$  stated by the Hot-Air-Blower system (Figure 7). For this reason, the temperature during the experiment was corrected using the linear regression function  $T_{cor} = 1.06251T_{HAB} - 7.37057$  obtained by fitting the temperature data assigned to the lattice parameter of silicon (Figure 8).

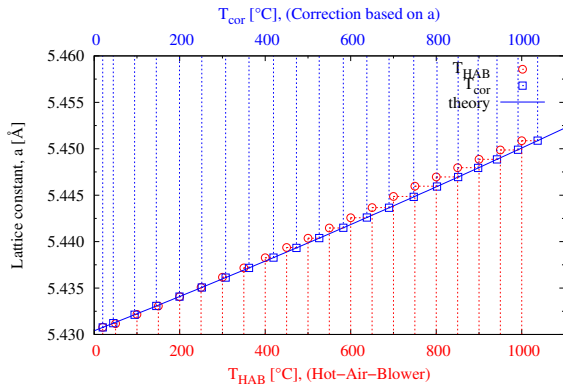


**Figure 7:** Comparison of the temperature  $T_{HAB}$  of the Hot-Air-Blower and the corrected temperature  $T_{cor}$  at the sample determined from the lattice parameter  $a$  of silicon

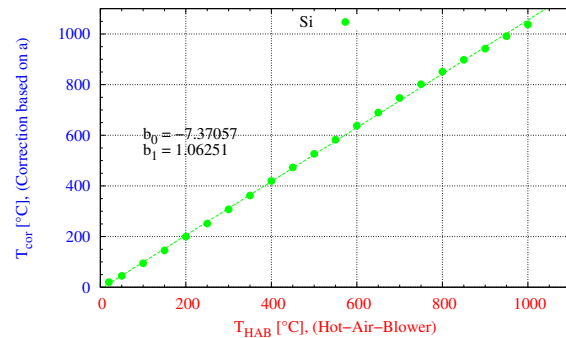


**Figure 8:** Corrected temperature  $T_{cor}$  as a function of the temperature  $T_{HAB}$  of the Hot-Air-Blower - linear regression fit

### 4.2 SBA-G57Fe1050-matrix

An example of the diffraction pattern of the sample SBA-G57Fe1050-matrix of  $\varepsilon$ -Fe<sub>2</sub>O<sub>3</sub> nanoparticles in the silica matrix is shown in Figure 9, after integration and background

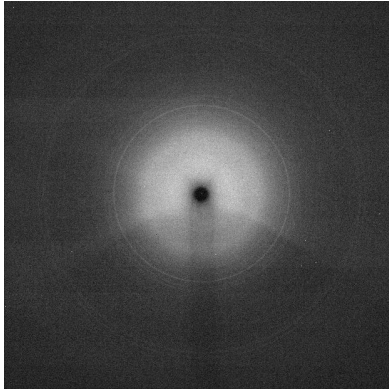


**Figure 9:** An example of a diffraction pattern of the sample SBA-G57Fe1050-matrix, air scattering predominates

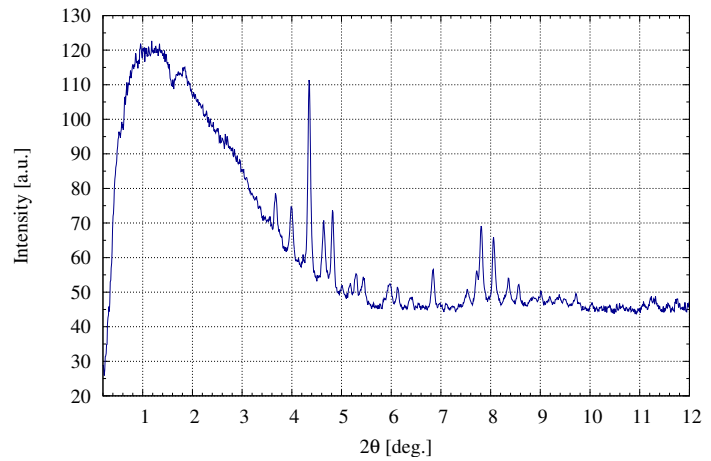


**Figure 10:** A diffractogram of the sample SBA-G57Fe1050-matrix,  $T_{cor} = 333.1^\circ\text{C}$

subtraction in Figure 10. Diffraction pattern is dominated by the amorphous peak of silica in the range of  $2\theta \sim 0.2 - 5$  degrees. It is apparent from the temperature dependence of the diffraction profile (Figures 11 and 12) that the phase composition of the sample does not change in the examined temperature interval. An example of a fitted diffractogram with Miller indices assigned to peaks is shown in Figure 13.

The temperature dependence of the relative change of the unit cell volume of  $\epsilon$ -Fe<sub>2</sub>O<sub>3</sub> is depicted in Figure 14, of the lattice parameters in Figure 15. Reference lattice parameters are  $a_0 = (5.098 \pm 0.003) \text{ \AA}$ ,  $b_0 = (8.813 \pm 0.009) \text{ \AA}$  and  $c_0 = (9.470 \pm 0.008) \text{ \AA}$  for  $T_0 = 46.3^\circ\text{C}$ . In general, the lattice parameters grow with increasing temperature, linear regression lines in the Figures 14 and 15 merely indicate the overall trend of the growth. The unit cell volume rises by up to 2 % during the experiment. However, both lattice parameters and unit cell volume changes with temperature exhibit a certain hysteresis differentiating between the process of heating up and cooling down the sample.

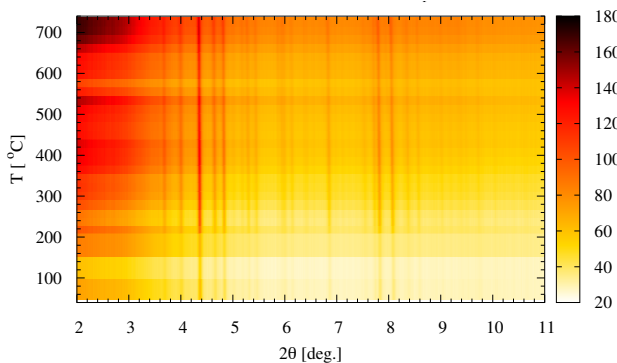


**Figure 11:** Temperature dependence of the diffraction profile of SBA-G57Fe1050-matrix during the heating

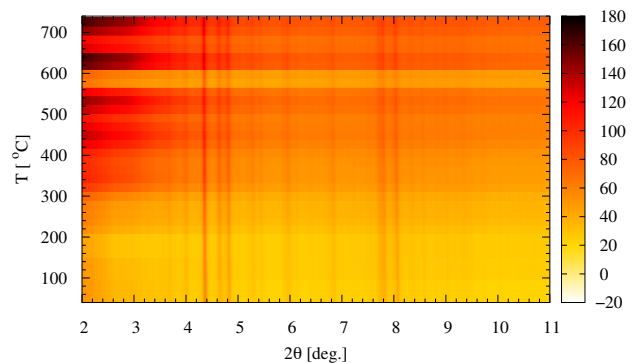


**Figure 12:** Temperature dependence of the diffraction profile of SBA-G57Fe1050-matrix during the cooling

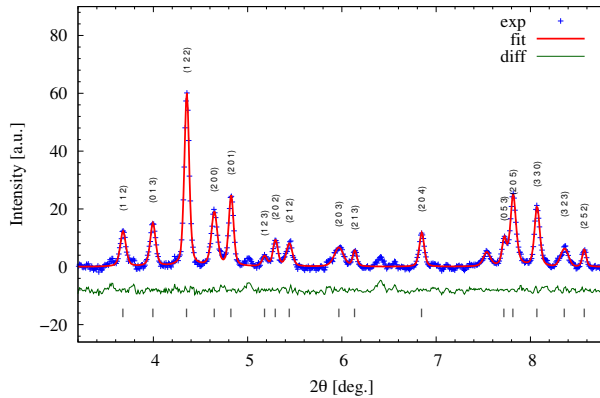


**Figure 13:** A fitted interval of the diffraction profile of SBA-G57FA1075-matrix with Miller indices

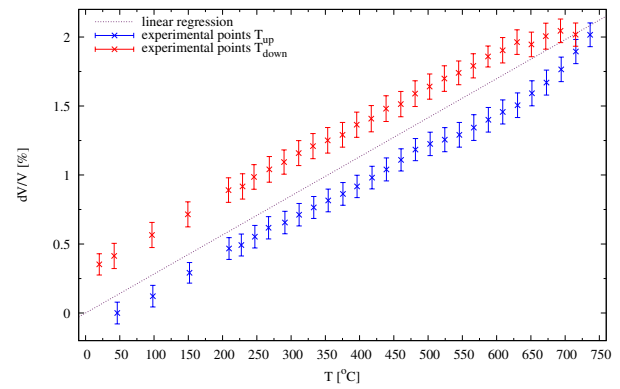


**Figure 14:** Temperature dependence of relative changes of the unit cell volume of  $\varepsilon$ - $\text{Fe}_2\text{O}_3$  nanoparticles in SBA-G57FA1075-matrix

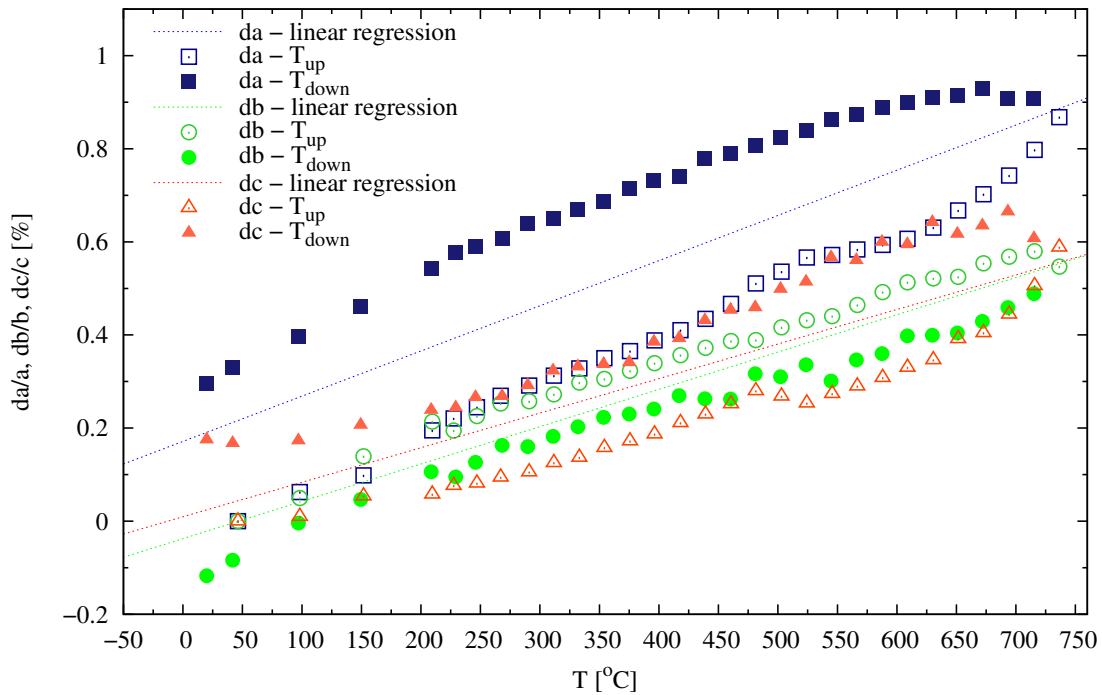


**Figure 15:** Temperature dependence of relative changes of lattice parameters of  $\varepsilon$ - $\text{Fe}_2\text{O}_3$  nanoparticles in SBA-G57FA1075-matrix

A certain change in the slope of the changes of lattice parameters occurred in the interval of temperatures  $\sim 450 - 550^\circ\text{C}$ , where the second sample SBA-G57Fe1050-NC1 underwent a phase transition to  $\gamma$ - $\text{Fe}_2\text{O}_3$ . No change in the lattice parameters that could be ascribed to a magnetic transition to the paramagnetic state at the Curie temperature  $\sim 220^\circ\text{C}$  stated in the literature (see [6]) was observed.



### 4.3 SBA-G57Fe1050-NC1

A temperature dependence of the diffraction profile of the sample SBA-G57Fe1050-NC1 consisting of bare  $\varepsilon$ -Fe<sub>2</sub>O<sub>3</sub> nanoparticles during the heating process is depicted in Figure 16. A phase transition from  $\varepsilon$ -Fe<sub>2</sub>O<sub>3</sub> to  $\gamma$ -Fe<sub>2</sub>O<sub>3</sub> occurs at the temperature interval 400 °C - 500 °C. The diffraction pattern of  $\gamma$ -Fe<sub>2</sub>O<sub>3</sub> (maghemite) is more simple due to its cubic crystal structure (described by a symmetry space group P4<sub>1</sub>32). For maghemite is a more stable phase of the ferric oxide, subsequent cooling of the sample produced no further change of the phase composition of the sample (Figure 17). The diffraction patterns, diffractograms and fitted profiles with assigned Miller indices of  $\varepsilon$ -Fe<sub>2</sub>O<sub>3</sub> and  $\gamma$ -Fe<sub>2</sub>O<sub>3</sub> are depicted in Figures Figures 18 to 23 for comparison. The lattice parameter  $a$  of maghemite decreases with decreasing temperature as shown in Figure 24, no demonstrable hysteresis was proved. Again, the linear regression in the Figure 24 only indicates the trend. No sudden changes in the slope of the lattice parameter increase were indicated.

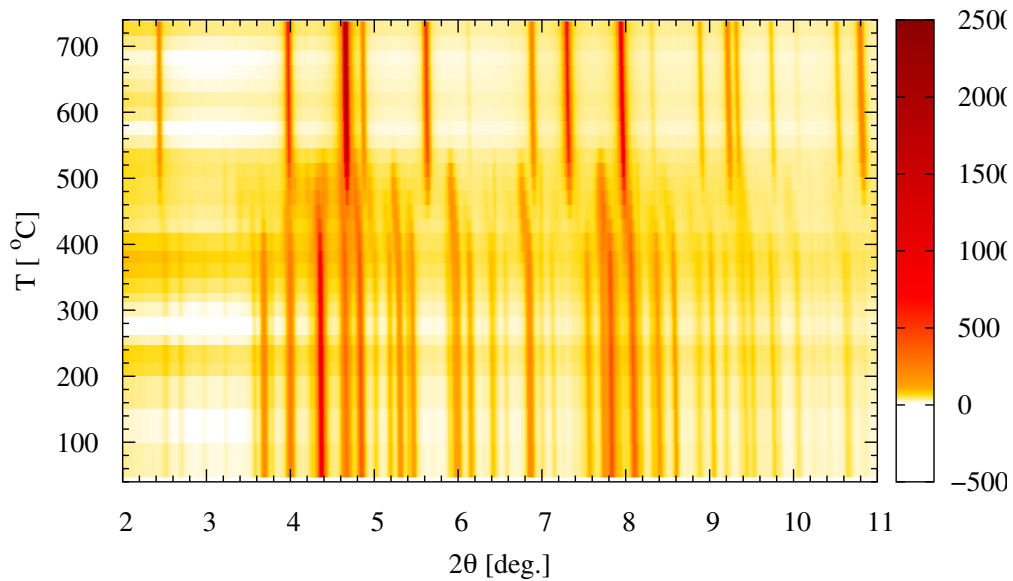


**Figure 16:** Temperature dependence of the diffraction profile of  $\varepsilon$ -Fe<sub>2</sub>O<sub>3</sub> nanoparticles in SBA-G57Fe1050-NC1 during the heating

## 5 Conclusions

The temperature dependence of lattice parameters of two samples of  $\varepsilon$ -Fe<sub>2</sub>O<sub>3</sub> nanoparticles was measured in situ using X-ray diffraction experiments at the beamline P02.1 of the PETRA III synchrotron radiation source. The sample SBA-G57Fe1050-matrix of nanoparticles in silica matrix remained in the epsilon phase for the examined temperature interval (Figures 11 and 12), while in the sample SBA-G57Fe1050-NC1 consisting

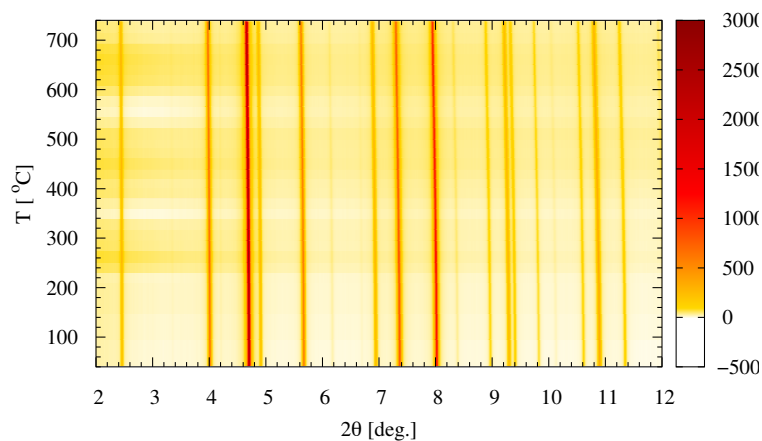


**Figure 17:** Temperature dependence of the diffraction profile of nanoparticles in SBA-G57Fe1050-NC1 during the cooling -  $\gamma$ -Fe<sub>2</sub>O<sub>3</sub>

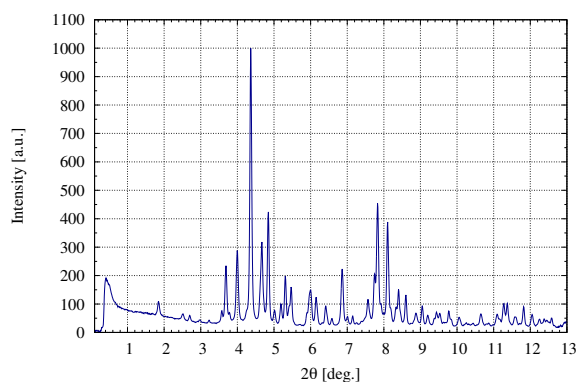


**Figure 18:** An example of a diffractogram of the  $\varepsilon$ -Fe<sub>2</sub>O<sub>3</sub> - sample SBA-G57Fe1050-NC1,  $T_{cor} = 47.1^\circ\text{C}$

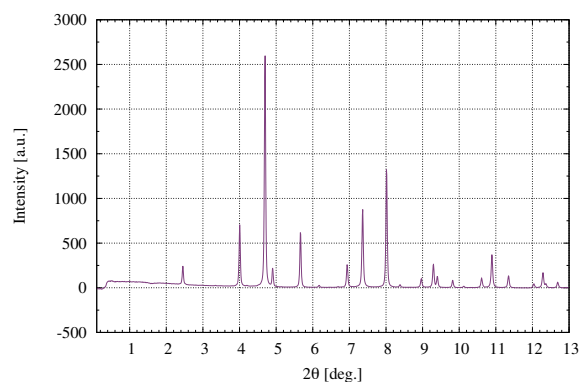


**Figure 19:** An example of a diffractogram of the  $\gamma$ -Fe<sub>2</sub>O<sub>3</sub> - sample SBA-G57Fe1050-NC1,  $T_{cor} = 20.0^\circ\text{C}$

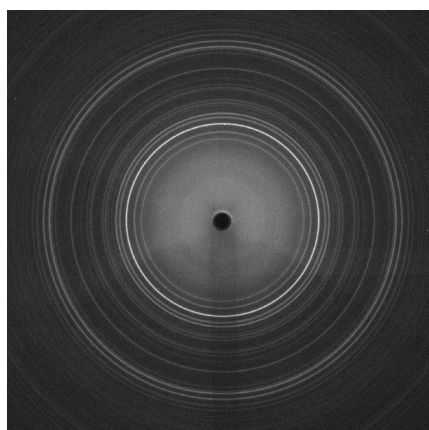


**Figure 20:** An example of a diffraction pattern of the  $\varepsilon$ -Fe<sub>2</sub>O<sub>3</sub> - sample SBA-G57Fe1050-NC1

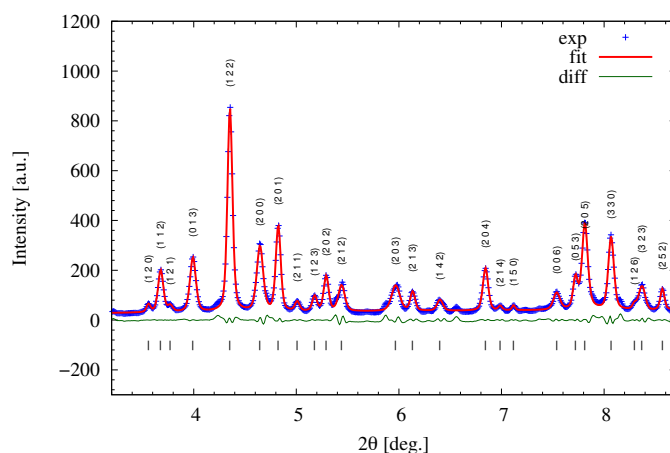


**Figure 21:** A fitted interval of the diffraction profile of SBA-G57FA1075-NC1 with Miller indices -  $\varepsilon$ -Fe<sub>2</sub>O<sub>3</sub>

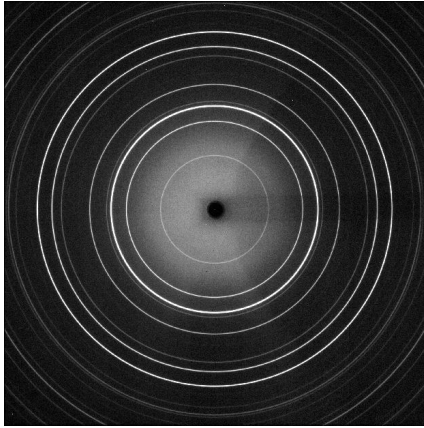


**Figure 22:** An example of a diffraction pattern of the  $\gamma$ - $\text{Fe}_2\text{O}_3$  - sample SBA-G57Fe1050-NC1

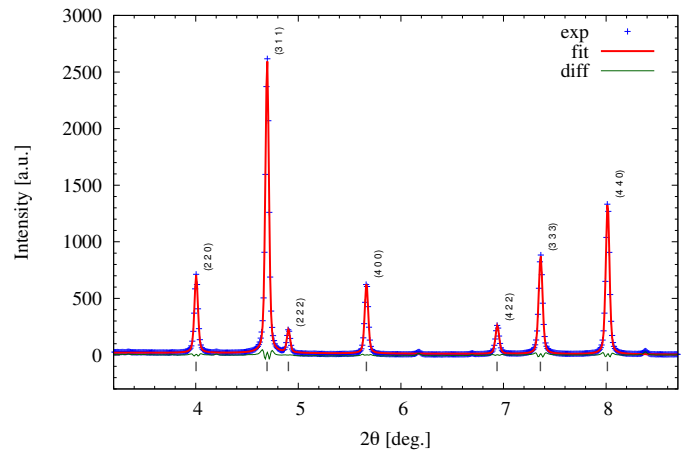


**Figure 23:** A fitted interval of the diffraction profile of SBA-G57FA1075-NC1 with Miller indices -  $\gamma$ - $\text{Fe}_2\text{O}_3$

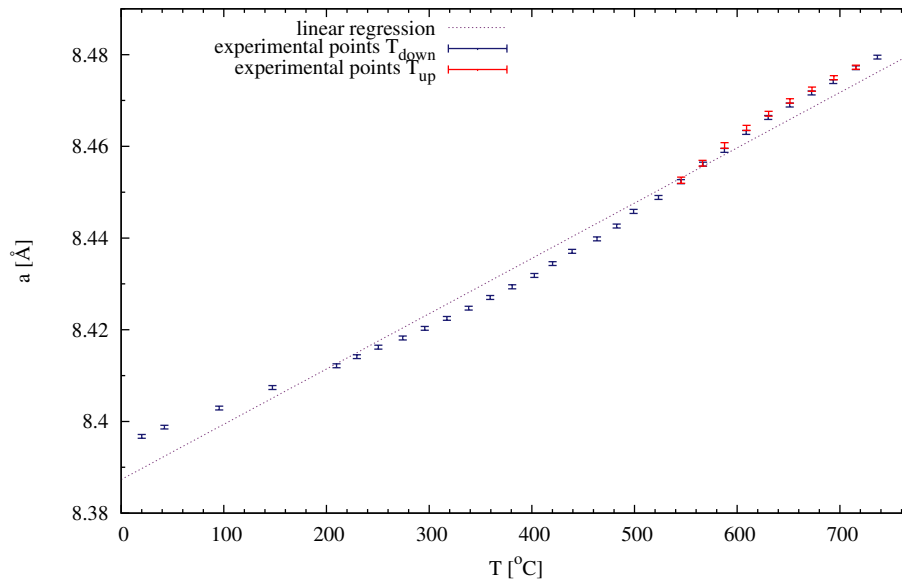


**Figure 24:** Temperature dependence of the lattice parameter  $a$  of  $\gamma$ - $\text{Fe}_2\text{O}_3$

of bare nanoparticles a transition to the gamma phase occurred inside the interval of temperatures  $\sim 400 - 500^\circ\text{C}$  (Figure 16). During the process of cooling the SBA-G57Fe1050-NC1 remained in the form of  $\gamma$ - $\text{Fe}_2\text{O}_3$  (Figure 17). Both lattice parameters and the unit cell volume of  $\varepsilon$ - $\text{Fe}_2\text{O}_3$  nanoparticles increase with rising temperature, exhibiting a certain hysteresis (Figures 15 and 14). The lattice parameter of  $\gamma$ - $\text{Fe}_2\text{O}_3$  also grows with rising temperature; nevertheless, no verifiable hysteresis as in the case of  $\varepsilon$ - $\text{Fe}_2\text{O}_3$  was observed (Figure 24).

## Acknowledgement

I would like to express my sincere thanks to Dr. Jozef Bednarčík and Jana Michalíková for their patience, willingness and kind approach. I also want to acknowledge DESY for the opportunity to participate in the Summer Student Program, and organisers, lecturers and all the participants for this amazing experience.

## References

- [1] Jiří Tuček, Radek Zbořil, Asuka Namai, and Shin-ichi Ohkoshi.  $\epsilon$ -Fe<sub>2</sub>O<sub>3</sub>: An advanced nanomaterial exhibiting giant coercive field, millimeter-wave ferromagnetic resonance, and magnetoelectric coupling. *Chemistry of Materials*, 22(24):6483–6505, 2010.
- [2] Klemens Kelm and Werner Mader. Synthesis and structural analysis of  $\epsilon$ -Fe<sub>2</sub>O<sub>3</sub>. *Zeitschrift für anorganische und allgemeine Chemie*, 631(12):2383–2389, 2005.
- [3] A. P. Hammersley. FIT2D V9.129 reference manual v3.1. Technical Report ESRF98HA01T, 1998.
- [4] W. Kraus and G. Nolze. POWDER CELL - a program for the representation and manipulation of crystal structures and calculation of the resulting X-ray powder patterns. *Journal of Applied Crystallography*, 29(3):301–303, Jun 1996.
- [5] Thomas Williams, Colin Kelley, and many others. Gnuplot 4.4: an interactive plotting program. <http://gnuplot.sourceforge.net/>, March 2010.
- [6] Jaroslav Kohout, Petr Brázda, Karel Závěta, Denisa Kubániová, Tomáš Kmječ, Lenka Kubíčková, Mariana Klementová, Eva Šantavá, and Adriana Lančok. The magnetic transition in  $\epsilon$ -Fe<sub>2</sub>O<sub>3</sub> nanoparticles: Magnetic properties and hyperfine interactions from Mössbauer spectroscopy. *Journal of Applied Physics*, 117(17):17D505, 2015.